

INSTRUMENTATION

A Boundary Method for Attenuation Correction in Positron Computed Tomography

Sung-Cheng Huang, Richard E. Carson, Michael E. Phelps, Edward J. Hoffman, Heinrich R. Schelbert, and David E. Kuhl

UCLA Medical School and University of California at Los Angeles, Los Angeles, California

A new method for attenuation correction in positron computed tomography (PCT) has been developed, and it can improve the quality of PCT images. The method requires a short transmission scan by the PCT system. Then boundaries between tissues with significantly different attenuation coefficients are determined from the transmission image by edge-finding techniques. Attenuation correction factors (ACF) are then calculated using these boundaries and the average attenuation coefficients within the enclosed regions. The method has been tested on computer-simulated data, on scans of phantoms, and on patient studies, and has been found effective in reducing the random noise in transmission measurements and in providing more accurate ACFs than the method using geometric attenuation correction. As a result, transmission scan times can be shortened, inconvenience to patients is reduced, and PCT images are improved.

J Nucl Med 22: 627-637, 1981

Positron computed tomography (PCT) requires accurate attenuation correction (AC) to give quantitative results (1-3). AC in PCT is normally accomplished by applying an attenuation correction factor (ACF) to each projection measurement in a scan. Two methods are commonly used today to obtain ACFs. The first uses transmission measurements (TM) of attenuation with external positron sources; the second uses calculations from simple geometric shapes that approximate the attenuating media. It has been shown (2,4) that random noise in TM can seriously increase the noise level of PCT images. Although the noise level in TM can be reduced by filtering, the amount of reduction is limited because excessive filtering will introduce serious image distortion (2). Thus, the TM method will not give accurate ACFs unless random noise in the TM is low. However, low-noise TMs require long scan times, which greatly increase the probability of patient motion and the amount

of patient discomfort. Although random noise in TM can also be avoided by using the geometric AC method, that method is subject to other problems. For example, no organ can be fitted exactly by geometric shapes. In addition, discrepancies in size, location, and attenuation coefficient could all introduce distortion in PCT images (2,5). Neither of the two AC methods is ideal.

We have developed a boundary method that can provide accurate AC without the need of low noise in TM. The method calculates ACFs from noise-free images that are extracted from noisy transmission images through a series of image-processing procedures. The method has been applied to computer-simulated PCT data, to scans of phantoms, and to brain and heart scans of patients, and has been found to improve PCT images.

DESCRIPTION OF BOUNDARY METHOD

The boundary method utilizes the transmission images to provide key features of attenuation in cross-sections of interest. From these features, noise-free transmission images are formed and ACFs that are free of random noise can be calculated. The method consists of a few

Received Dec. 19, 1981; revision accepted March 13, 1981.

For reprints contact: Sung-cheng Huang, DSc, Div. of Nuclear Medicine, UCLA Medical School, 405 Hilgard Ave., Los Angeles, CA 90024.

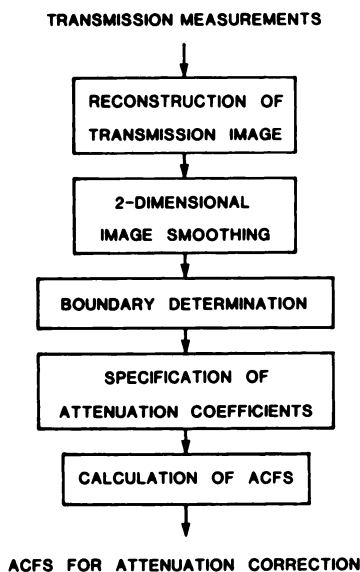


FIG. 1. Block diagram illustrating various processing steps in boundary method. For details of each step see text.

image-processing steps, as illustrated in Fig. 1. First, a series of short TMs are performed on the patient, giving transmission images with high noise levels. The transmission images are then smoothed, and edge-finding techniques are used to find boundaries between tissues with major differences in attenuation. After boundaries are located, each region enclosed by a boundary is assigned a uniform attenuation coefficient equal to the average value within that region of the original transmission image. In other words, the image is quantized into a few discrete levels of attenuation coefficients. ACFs at all angular views can then be calculated from the quantized image. Through these operations, the random noise of the original TM is removed. Each of the image-processing steps is described separately in the following.

Two-dimensional smoothing. Initially, transmission images are smoothed by a two-dimensional filter to reduce image noise level. Figure 2 shows a filter that is normally used. The smoothing operation can be applied to an image repeatedly. After each smoothing operation, the smoothed image is displayed and the operator decides whether or not to repeat the operation. Usually no more than two smoothing operations are necessary. After the smoothing, boundaries can be obtained more easily by the edge-finding techniques.

Boundary determination. Boundaries between regions with significant differences in attenuation can be drawn by the operator using a joystick interfaced to the video display unit. However, in order to reduce the amount of operator interaction and to reduce the dependence on operator judgment, an edge-finding computer program has been developed to locate the boundaries. In this program, edge-enhancement techniques are first applied to the smoothed image, and an edge tracing algorithm

.011	.021	.033	.021	.011
.021	.049	.083	.049	.021
.033	.083	.130	.083	.033
.021	.049	.083	.049	.021
.011	.021	.033	.021	.011

FIG. 2. Typical two-dimensional filter used for image smoothing to facilitate boundary determinations by edge-finding techniques.

is used on the edge-enhanced image to find continuous and closed boundaries. Currently we use the Laplacian method (6) for edge enhancement. The

Laplacian $\left(\frac{\partial^2}{\partial x^2} + \frac{\partial^2}{\partial y^2}\right)$ is calculated by

$$\begin{aligned}
 & [(a_{i+1,j} - a_{i,j}) - (a_{i,j} - a_{i-1,j})] \\
 & + [(a_{i,j+1} - a_{i,j}) - (a_{i,j} - a_{i,j-1})] \\
 & = (a_{i,j-1} + a_{i-1,j} + a_{i+1,j} + a_{i,j+1}) - 4a_{i,j},
 \end{aligned}$$

where a_{ij} is the image value at pixel (i,j) and the other values of a are the image values of the immediately adjacent pixels. The edge-tracing algorithm is initiated by the operator's specifying a starting point on an enhanced edge. The neighboring pixel that has the minimum Laplacian value is then chosen as the next edge point. This selection operation is repeated for the newly chosen edge point until the edge points thus chosen form a closed boundary. To reduce the influence of image noise, the edge-point selection is restricted so that sharp changes in direction and large changes in Laplacian values are not allowed. Infrequently a "dead end" can occur, if a subsequent edge point cannot be found under the specified restrictions. When this happens, the tracing can be continued either by direct operator selection of the subsequent point or by relaxing the restrictions. The tracing can also be restarted by relocating the starting point.

The number of boundaries needed depends on the image complexity and the attenuation heterogeneity of the image. Normally two boundaries are required for brain images and six or more for chest images. Occasionally a boundary between two adjacent regions is known to exist in anatomy, but because of small object size or low imaging resolution, the image contrast may be too low to yield a sharp edge. In such cases, a thresholding method, which adds a fixed value to all pixels that have attenuation above the threshold value, is used to increase the image contrast between the regions before starting the edge enhancement.

The jitter in boundaries due to the noise in the edge-enhanced image can be reduced further by performing separate smoothings on the x and y coordinates of the edge points along each boundary. Capability for interactive operator editing of the boundaries is also provided to ensure the boundaries are satisfactory.

Specification of attenuation coefficients. Within each region enclosed by a boundary, a uniform attenuation coefficient is assigned, equal to the average value within the region in the original image. Specification of these internal points is accomplished by first defining all intersections of the boundary with the columns of the image. Enclosed pixels are then read off column by column between points of intersection. Corrections for crossovers of attenuation between adjacent regions, due to imaging resolution, are accomplished by the technique described in the Appendix.

Calculation of projections and ACFs. After values of attenuation coefficients have been assigned, the image consists of only a few discrete levels, and ACFs can be calculated by projecting the quantized image at all angles. The projection at each location is calculated by first finding the intersecting points of the projection line and the boundaries. Each segment between two adjacent intersection points is then weighted by its length and by the appropriate attenuation coefficient. The corresponding ACF is the exponential of the weighted sum of all the segments of the projection line.

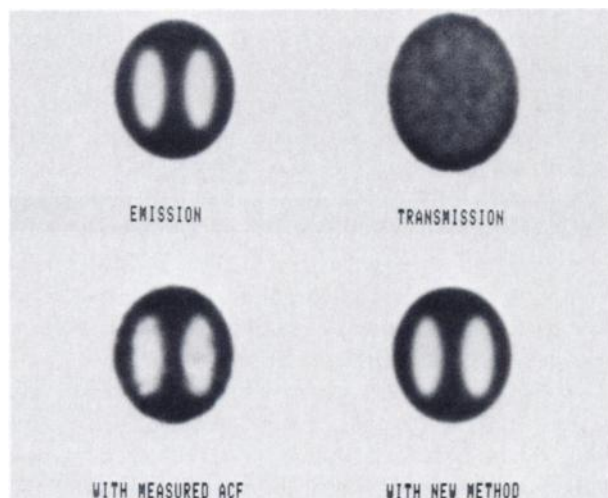


FIG. 3. Images of computer-simulated data. Simulated head slice consisted of elliptical structures. Dimensions of head were 18 cm vertical by 15 cm horizontal. Skull varied from 0.8 cm thick in front to 1.2 cm in back, $\mu = 0.154 \text{ cm}^{-1}$; brain $\mu = 0.088 \text{ cm}^{-1}$. Two radioactivity levels (relative concentrations 20 and 7) were in brain tissue to simulate gray and white matter. Pseudorandom noise corresponding to 7.2 M counts was added to simulate transmission measurements (image at upper right); no noise was added to emission scan data. Upper left shows emission image attenuation-corrected with noiseless transmission measurements; lower left shows same using noisy transmission measurements. Image noise was eliminated completely by boundary method, as shown at lower right. No apparent artifacts were generated by new method.

The sharp discontinuities created by the boundaries separating discrete levels of attenuation are smoothed by filtering the ACFs along the transverse direction with a resultant resolution comparable to the original transmission measurements.

All the processing steps have been implemented on a computer of an ECAT system (7). The computer's processing times for these four steps vary from image to image. Nominally they take about 5, 15, 60, and 30 sec, respectively, but more time is usually required for interactive operations.

METHODS AND MATERIALS

The boundary method was tested on computer-simulated PCT data, on scans of phantoms, and on actual patient scans. All the scans on phantoms and patients were obtained with an ECAT scanner. Standard shadow shields (7) and a medium-resolution reconstruction filter (7) were used for phantom and brain scans; low-resolution shadow shields (7) and a low-resolution filter were used for heart studies, unless otherwise stated.

Computer-simulated PCT data. The method of computer simulation has been described previously (2). Two object configurations (one corresponds to a brain section and one to a chest section) were simulated. The detail configurations are described in the captions of Figs. 3 and 4. In the simulation, the intrinsic full widths at half maximum (FWHM) of the detector's response function

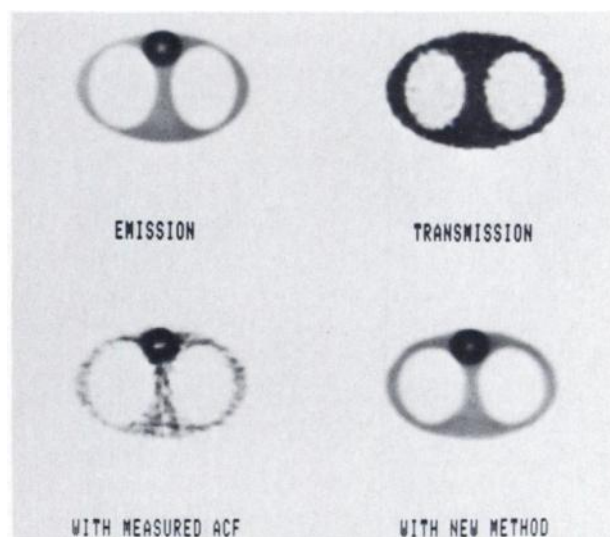


FIG. 4. Images of computer-simulated chest section, 36 cm wide and 24 cm high. Two lungs had $\mu = 0.022 \text{ cm}^{-1}$, other tissue had $\mu = 0.088 \text{ cm}^{-1}$. Radioactivity concentrations in myocardium, in chest tissue, and in lungs were 150, 50, and 10, respectively. Noise corresponding to 14 M counts was added to simulated transmission data; no noise was added to emission data. Upper right shows transmission image. Upper left shows emission image corrected with noiseless transmission measurements; lower left is emission image using noisy transmission measurements for AC. Lower right image is result of boundary method, which is clearly effective in eliminating random noise in transmission measurements.

were chosen to be 1.3 and 2.0 cm, respectively, for the brain and chest sections, and for the reconstructions the medium-resolution filter of the scanner was used for the former and the low-resolution for the latter. Both the emission and transmission scans were simulated. The emission scans were free of noise, whereas random noise corresponding to 7.2 and 14 million (M) counts, respectively, were simulated in the transmission scans of the brain and chest section. The new method was then applied to the transmission images to obtain the boundaries, and the resultant attenuation coefficients were compared with the simulated values. Emission images corrected by the calculated ACFs were compared with images that used ideal ACFs, and with images that used the noisy transmission measurements directly.

Scans on phantoms. Two phantoms were used. One was cylindrical, 20 cm in diameter, corresponding approximately to the size of a head section. Three separate compartments of the phantom, as shown in Fig. 5, were filled with water, and the rest contained air. Two transmission scans, giving 3 M and 30 M counts, were made on the phantom. Then water in the phantom was replaced by a Ga-68 solution, and the phantom was returned to the same position for an emission scan (6.6 M counts). The boundary method was then applied to the transmission scan of 3 M counts. The emission image resulting from the new method was compared with that using TM directly.

The other phantom simulated a human chest. Dimensions of the two axes were approximately 36 and 24 cm, respectively. Two styrofoam blocks inside the

phantom were used to simulate lung tissue, and three bottles, 1 in. in diameter, were used for gross simulation of the heart. The phantom was first filled with water, and two transmission scans (3 M and 27 M counts) were made. The water in phantom was then replaced by Ga-68 solution, and that in the three bottles with Ga-68 at a concentration about three times that of the outside solution. The phantom was returned to the same position for an emission scan (8 M counts). The boundary method was applied to the transmission image of 3 M counts, and the emission image obtained was compared with those using TM directly.

Brain studies. On one subject, a high-count (13 M) transmission scan and a low-count one (3 M) were made on a brain section of OM + 5 cm. An i.v. bolus injection of [^{18}F]fluorodeoxyglucose (FDG) was given, and 45 min later an emission scan (2 M) was made to obtain information related to the cerebral metabolic rate of glucose (8,9). Separate ACs were made by the boundary method, by direct TM, and by the geometric method. For the last we used an attenuation coefficient of 0.088 cm^{-1} , corresponding to the soft-tissue value.

On another subject, a head holder was used to restrain head movement and to help in repositioning the head between transmission and emission scans (10). Blank scans (7), with and without the head holder in place, were taken in advance. A transmission scan (20 M) was then made at OM+4 cm. Again, FDG was injected and an emission scan (2.5 M) was taken. The boundary method was applied to the transmission image to obtain ACFs of the brain slice. Attenuation due to the head holder was also obtained by taking the ratio between the two blank scans. AC on the emission scan was made in the following ways: (a) with TM directly, (b) with boundary method, (c) with boundary method plus compensation for head holder, and (d) with geometric AC. Emission images corresponding to different AC methods were then compared and quantitative values within the same regions of interest (ROI) in different images were taken for comparison.

Heart studies. On a normal subject, a transmission scan (13 M) of the chest was made. After i.v. injection of N-13 ammonia, an emission scan (1.4 M counts) was taken to show local myocardial perfusion (11,12). The boundary method was applied and emission images by different AC methods were compared. Emission images were also reconstructed with the medium-resolution filter for comparison.

A second patient with extensive myocardial infarction was scanned, and FDG was used to label the functioning capability of myocardium (13,14). Ten million and 1 M counts were obtained, respectively, for transmission and emission scans. The boundary method was applied and emission images with the new method were compared with those that used direct transmission measurements.

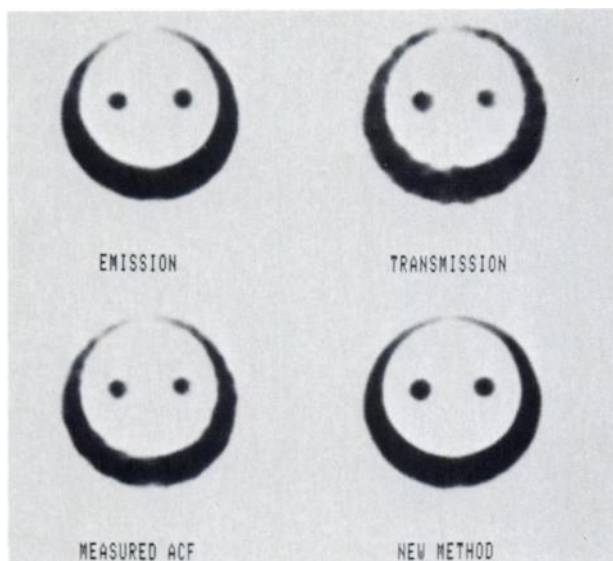


FIG. 5. Images of head phantom. Transmission image (3 M counts) is shown at upper right. Dark areas of image contain water; the rest contains air. Upper left shows emission image with Ga-68 in water; emission gave 6.6 M counts and image was corrected with measured ACFs of 13 M counts. Noisier image at lower left was from same emission data, corrected with measured ACFs of 3 M counts. This noise was reduced by boundary method as shown at lower right.

A third patient was scanned to test the applicability of the new method for low-count transmission images. In addition to the normal (5 min) transmission scans (7 M counts), a 2-min transmission scan (2.5 M counts) was made. Nitrogen-13 ammonia was injected and a 1-M-count emission scan was taken. The boundary method was applied to the low-count transmission image, and the emission image obtained was compared with those using TM directly.

RESULTS

Computer-simulated data. The boundaries obtained by the edge-finding technique were found to be within 1 pixel (2.5 mm for head simulation and 3.5 mm for chest) of the simulated configurations. The only exception is the boundary between the skull and the brain. Because the FWHM for the brain's transmission image was larger than the simulated skull thickness, the skull thickness on the image was approximately equal to the FWHM of the image due to the limitation of image resolution (15). As a result, the inside skull boundary obtained by the edge-finding technique was smaller than what had been simulated.

The attenuation coefficients for soft tissues and skull, as obtained by the boundary method, were 0.0885 cm^{-1} and 0.117 cm^{-1} , respectively. The latter is $\sim 24\%$ lower than the simulated value of 0.154 cm^{-1} . The smaller attenuation coefficient was compensated by the larger thickness of the skull, so the total attenuation was still

close to the values found by transmission measurements.

Figures 3 and 4 show the images of the simulated sections. The images with the boundary method are seen to be very close to the simulated configurations (also shown in the figures). Direct subtraction of one image from the other shows that the only noticeable difference between the two occurs near the boundaries, due to inexactness of the edge-finding process in assigning the boundaries. Such differences were smaller than 7% of the radioactivity in soft tissues. Average radioactivities in various regions of interest in the images obtained by the boundary method were within $\pm 2\%$ of the simulated values. A visual comparison with the images that used noisy transmission measurements shows that the random noise due to transmission measurements is effectively eliminated by the boundary method.

Scans on phantoms. Figures 5 and 6 show the images of the two phantoms. Those made by the new method are seen to be comparable to the images made with high-count transmission measurements. The differences in image-pixel values in various regions between the two images were found to be less than 4%. In general, the image-pixel values obtained with the boundary method are slightly lower, probably due to the small attenuation of the scanner bed that was not taken into account by the boundary method. The image noise levels as measured by the standard deviations of image-pixel values within various regions of interest were found to be comparable between images by the boundary method and by the high-count transmission measurements. The noise levels in the images that were attenuation-corrected with low-count transmission measurements were about twice as high on both the head-size and the chest-size phantoms. This noise increase due to transmission measurements is consistent with values predicted from the counts in the transmission and emission scans according to formulas previously reported (2). The noise-suppression capability of the boundary method is also quite apparent when the images of the boundary method are compared with those using low-count transmission measurements.

Brain studies. It was found that usually only two boundaries were needed: one on the outside of the skull and one on the inside. The edge-finding technique had no difficulty in finding the outside skull boundaries. Getting the inside boundary was more difficult because the image resolution was wider than the thickness of skull, which caused a contrast reduction between the skull and brain tissues (15). Usually the thresholding method was needed to enhance the image contrast between the skull and brain. Because of this limitation of image resolution (15), the distance between the two boundaries was close to the FWHM of the imaging resolution, which was usually larger than the true skull thickness. The attenuation coefficients for skull and

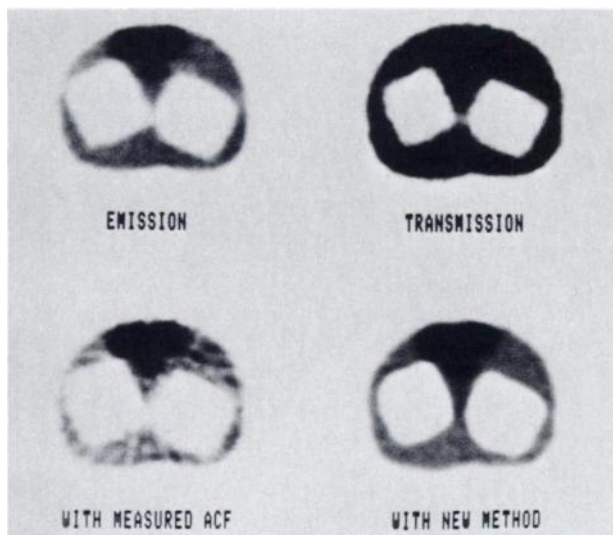


FIG. 6. Images of chest phantom, with lungs simulated by two styrofoam blocks. Upper right shows transmission image (3 M counts). Upper left shows emission image after water in phantom was replaced by Ga-68 solution, and after water in three 1-in. bottles was replaced by Ga-68 solution at ~ 3 times outside concentration. Image was from emission scan of 8 M counts and was corrected with measured ACFs of 27 M counts. Lower left image is from same emission data but using ACFs of 3 M counts directly for AC. Higher noise level due to transmission noise was removed effectively by boundary method, as shown at lower right.

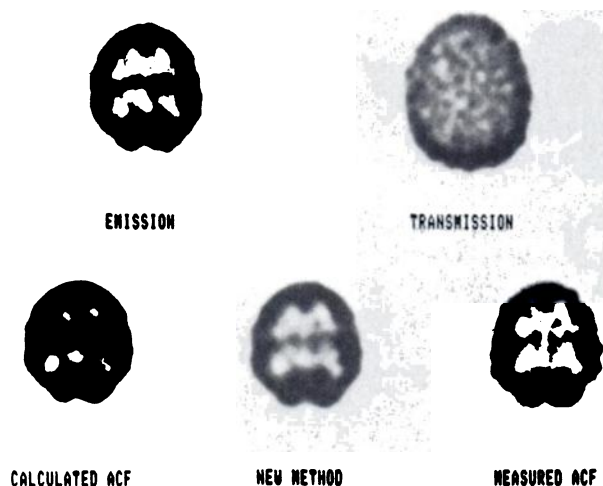


FIG. 7. Images from brain FDG study. Upper right is transmission image (3 M counts) of brain at OM + 5 cm. Upper left is emission image (2 M counts) corrected with a set of low-noise measured ACFs (13 M counts) to show true radioactivity distribution in slice. Lower right is image from same emission data but corrected with ACFs corresponding to image at upper right; image quality was seriously degraded by noise in ACFs. By using boundary method (bottom center) this noise was removed, giving image very close to control at upper left. Lower left came from same emission data but geometric AC was used. Lower reconstructed radioactivity in occipital cortex as compared with frontal is believed due to higher attenuation in occipital skull (cf., upper right), which has not been considered by geometric AC method.

brain tissue were found to be 0.110 and 0.089 cm^{-1} , respectively. The attenuation coefficient for skull was lower than that expected from a consideration of its density (1.7 times tissue) (16) and was believed to be compensating for the overestimation of the skull thickness to keep the total attenuation equal to the transmission measurement values.

Figure 7 shows images from a brain FDG study, the images being reconstructed with various AC methods. The upper left image was attenuation-corrected with a set of low-noise-measured ACFs, and serves as a control for comparison with other images. Qualitatively, the image by the boundary method (lower center) is closest to the control. The lower-right image used measured ACFs for AC, and although the same emission and transmission data were used, as at lower center, the method of directly using measured ACFs has introduced more noise in the image, and real brain structures are less easily distinguished from the random noise. The image by geometric AC (lower left) has a low noise level, but it shows the FDG concentration in the occipital cortex as lower than in the frontal cortex, whereas other images show comparable concentrations in those regions. The discrepancy is believed due to the higher attenuation in the occipital skull bone, which was not taken into account by the geometric AC method. When applying this method, we used the transmission image (upper right)

TABLE 1. COMPARISON OF QUANTITATIVE VALUES OF BRAIN IMAGES CORRECTED BY DIFFERENT METHODS OF ATTENUATION CORRECTIONS

Brain regions	Brain slice 1			Brain slice 2			
	Measured ACFs	New method	Geometric ACFs	Measured ACFs	New method		Geometric ACFs*
					Consider headholder	Ignore headholder	
Frontal cortex	1479 [†]	13885 (-6) [‡]	12800 (-13)	18697	19034 (2)	17065 (-9)	14201 (-24)
Temporal cortex	14291	13409 (-6)	11813 (-17)	18996	19681 (4)	17113 (-10)	14768 (-22)
Occipital cortex	13669	12498 (-8)	10181 (-25)	19439	20690 (6)	16438 (-15)	13503 (-31)
Subcortical [§] ganglia	10368	10473 (+1)	9605 (-7)	17287	16645 (-4)	15171 (-12)	14820 (-14)
White matter near front	9835	9365 (-5)	8857 (-10)	12549	11988 (-4)	11116 (-11)	10542 (-16)
White matter near back	9331	8859 (-5)	7985 (-14)	14177	13421 (-5)	11911 (-16)	11621 (-18)
Whole brain slice	10441	10275 (-2)	9356 (-10)	17275	17122 (-1)	14986 (-13)	13581 (-21)

* Attenuation due to the headholder has also been ignored in calculating the geometric ACFs.

[†] Number represents average value of image pixels in region of interest. Its unit is arbitrary but is kept the same for images using different AC methods.

[‡] Value in parentheses is enhancement or suppression in percentage of the mean values as compared with the corresponding values in image of measured ACFs.

[§] Represents a region of interest, about $6 \times 4 \text{ cm}$, near the center of the brain slice. No attempt was made to separate gray matter from white within the ROI.

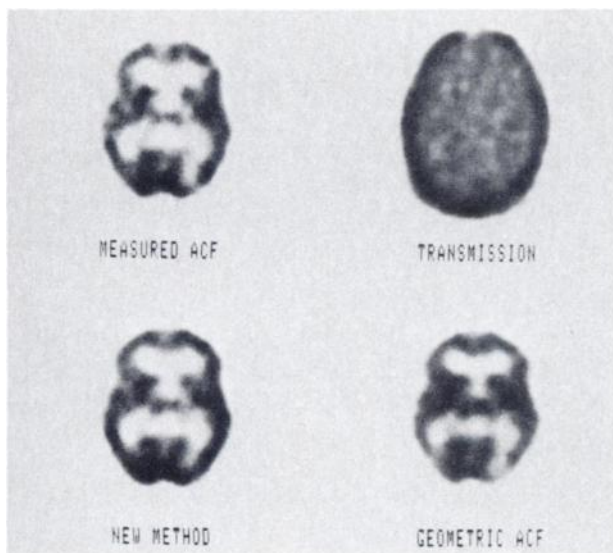


FIG. 8. Images from another FDG study. Upper right shows transmission image (20 M counts) of brain at OM + 4 cm. Upper left is emission image (2.5 M counts) corrected with measured ACFs corresponding to upper right image. Lower left was by boundary method, lower right by geometric AC method. Qualitatively the three emission images are similar, although reconstructed radioactivities by geometric AC method are much lower than values from other two images (see Table 1).

to guide the positioning of the ellipse. Thus, the artifact of uneven concentration is not caused by the malpositioning of the ellipse, although this could produce a similar artifact (2).

A comparison of quantitative values in a few ROIs among different images is shown in Table 1 under the column headed Brain slice 1. Values by the boundary method are seen to be very close to those by the measured ACFs. Some of the differences in values between the new method and the measured ACFs are believed to be due to the attenuation of the patient's bed, which has not been taken into account by the boundary method. Values by the geometric method are much too low. In general, the geometric AC method causes suppressions of about 17, 7, and 10%, respectively, in cortical regions, in sub-cortical regions, and over the whole brain slice. These amounts of suppression are consistent with values previously reported, if the higher attenuation of skull is not considered (2).

Figure 8 shows images from another FDG study that had used a head holder to avoid movement of the head during the scan. Qualitatively, the images with different AC methods are comparable. However, as shown by the ROI values in Table 1 for Brain slice 2, if the head holder and the patient's bed were ignored in AC, a -10 to -15% error would be introduced in the reconstructed radioactivity. When the head holder and the bed were considered, the boundary method gives values very close to those by the measured ACFs. The geometric AC method again gives values much lower than with the other

methods. The amounts of suppression are larger than those in Brain slice 1, because neither the head holder nor the higher attenuation of the skull was considered in the geometric attenuation correction.

Heart studies. At least six boundaries were needed to separate regions with different attenuation coefficients in a transmission image of the chest: one for the skin surface, two for the lungs, one for the spinal column, and two for the arm bones. As in the brain studies, the finite image resolution imposed some limitations on getting the exact boundaries of the regions. Usually, the assigned boundaries for the spinal column and arm bones were larger than their anatomical sizes. The chest walls specified by the boundaries were also thicker than they should be. However, these overestimations were compensated by the lower attenuation coefficients calculated for those regions. The attenuation coefficients for bone and soft tissues were found to be about 0.105 cm^{-1} and 0.084 cm^{-1} , respectively. The attenuation coefficient of the lung tissue ranged from 0.02 cm^{-1} – 0.04 cm^{-1} .

Figure 9 shows images of an N-13 ammonia study of the heart. At upper left is the transmission image, showing the lower attenuation of lung and the higher attenuation of bony structures (spine and arm) in a typical chest cross section. At upper middle is the emission image that was attenuation-corrected with the measured ACFs. Upper right is the emission image by the boundary method, and it contains no obvious artifacts. Quantitatively, the reconstructed radioactivities

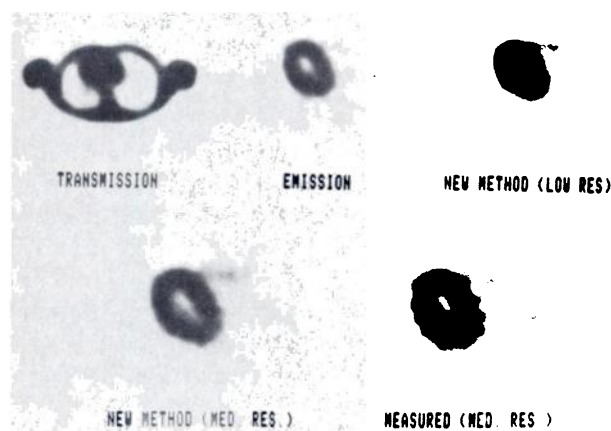


FIG. 9. Images from N-13 ammonia study on heart. Upper left is transmission image (13 M counts) of chest. Upper middle is emission image (1.4 M counts) corrected with measured ACFs directly. Upper right used same emission and transmission data but boundary method was used for AC. The two emission images are very similar, both qualitatively and quantitatively. Because low-resolution reconstruction was used and transmission scan already had fairly high counts, noise improvement with new method was not very significant. However, when the same images were reconstructed with medium-resolution filter, noise-reducing capability of boundary method becomes more obvious, as shown by two lower images. Note that no apparent artifacts were created by boundary method.

in myocardium on the two emission images are found to be within 5% of each other.

The lower two images are similar to the upper ones except that they were reconstructed with the medium-resolution filter of the PCT system and were zoomed up to show more details in the images. The noise level in the images with measured ACFs becomes higher with the medium-resolution filter and is also seen to be higher than in the image with the boundary method. Although there is no drastic improvement in image resolution with the medium-resolution filter—because the emission-scan data were taken with low-resolution shadow shields, which limit the recoverable image resolution—the method's lower noise level provides a good potential for resolution improvement in other scanning environments (e.g., when medium- or high-resolution shadow shields are used).

For the FDG study on a patient with extensive myocardial infarction, the image by the boundary method was also found comparable to that using measured ACFs, as shown in Fig. 10. It shows that the method is useful in diseased conditions.

The capability of the new method in a high-noise environment is demonstrated by the images shown in Fig. 11. The image by the boundary method is seen to have lower noise levels than those in the two images by measured ACFs. The transmission image at lower right was reconstructed from the ACFs that were calculated by the boundary method. When compared with the original transmission image at lower left, it clearly shows that the new method can effectively remove all the random noise in a transmission image while still retaining the basic features of the image.

DISCUSSION

As shown by the reconstructed emission images, the boundary method can effectively reduce random noise in transmission measurements. Although extensive smoothing on the noisy transmission measurements can

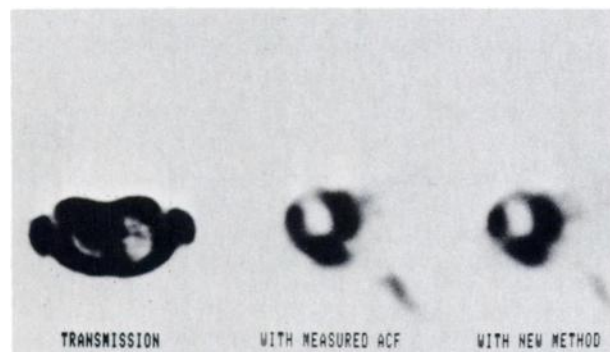


FIG. 10. Images of FDG study on patient with extensive myocardial infarction. Left is transmission image (10 M counts). Middle is emission image (1 M counts) by measured ACFs. Right is emission image by boundary method. Similarity between two emission images indicates applicability of boundary method in disease.

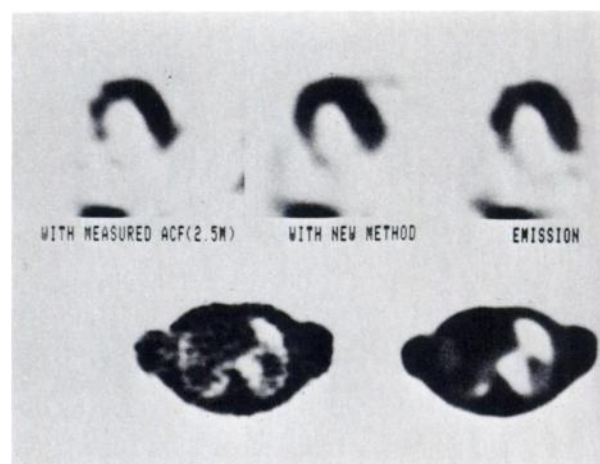


FIG. 11. Images of ammonia study to show applicability of boundary method for low-count transmission scans of chest. Subject has perfusion deficiency in posterior wall of the heart. Upper left is emission image (0.9 M counts) corrected with measured ACFs of 2.5 M counts. Upper center image was with boundary method. Upper right image was corrected with measured ACFs of lower statistical noise (7 M counts). Lower left is transmission image of 2.5 M counts. Lower right is transmission image reconstructed from ACFs that were calculated from boundary method. New method clearly shows dramatic noise reduction without loss of key features in transmission image.

also reduce transmission noise, it could seriously degrade image resolution and cause image artifacts (2). Unlike the method of simply smoothing the transmission measurements, the boundary method, when applied to a wide variety of object configurations, has not created any serious image artifacts or resolution losses and has provided images very close to the control images, both qualitatively and quantitatively. In other words, the boundary method has been shown to be capable of improving PCT images. However, the new method still has some limitations. For example, the imaging resolution of PCT has limited the capability of the edge-finding technique in locating the exact boundaries for regions that have dimensions smaller than the FWHM of the imaging resolution. However, because the attenuation coefficient for each region is obtained directly from the transmission images, the errors made on the boundaries are partially compensated by the values of the attenuation coefficients. The net effect on the ACFs is not as severe as one would have predicted by considering the boundary errors alone. This is shown by the close similarities between emission images by the boundary method and by the use of the transmission measurements. The boundaries can also be edited interactively, if necessary, to match the known anatomical sizes better. This has not been explored extensively, however, because the boundary errors have not created serious problems for the brain and chest images examined in the present study. Also, this resolution limitation problem is expected to be reduced as PCT resolution is gradually improved (17).

The boundary method is still subject to errors introduced by movement of the subject between the times of transmission measurements and emission scans (2). Although the shorter scan time for TM reduces the chance of gross movement, it does not eliminate the problem completely. For brain studies, the use of a head holder can avoid this problem. As shown in the results of Table 1, the extra attenuation due to the head holder needs to be taken into account to avoid large quantitative errors.

The boundary method goes through a series of image-processing steps. Each of these takes time, especially the boundary-determining step, which requires some operator interactions. Thus, the new method will lengthen the total image reconstruction time. In most cases, however, the only interaction required is the selection of the starting points for the edge-tracing routine. The amount of time and skill required is usually comparable to that needed for performing the geometric AC method; extensive operator interaction is seldom required. Although, it is conceivable that carelessness in performing the boundary-determining step would cause unnecessary inaccuracy or artifacts in the reconstructed image (2), we find that the final image is quite insensitive to small errors in determining the boundaries. We are continuing to evaluate other edge-finding techniques. We hope to find a technique that is independent of factors, such as image resolution and object size, and needs even less operator interaction than the present one. Also, potentially, when a high-speed array processor is used, the processing time required for the boundary method would be much reduced.

The applicability of the boundary method to high noise is shown for both brain and heart studies. Compared with the method of using measured ACFs, the number of photon counts required by the boundary method for transmission measurements can be reduced by a factor of about 3–10 and still give comparable images. However, the minimal number of counts required is not clear. It will need more experience and investigation to find the answer. Even with the current reduction factor of 3–10 in count requirements, the transmission measurements for a six-plane heart study, which used to take 30–60 min on our PCT scanner, can now be completed in about 10 min. For brain studies, the ROI values in Table 1 show that the geometric AC method could cause large errors in the reconstructed radioactivity. Although ROI values are compared in only two brain slices, and there are large variations in the size, thickness, and attenuation of human skulls, the data nevertheless have revealed the basic problem of the geometric AC method and have indicated its inadequacy for true quantitative PCT measurements. If the boundary method is used, on the other hand, the transmission scans for a brain study of six planes will need only about 10 min with an ECAT scanner and will not cause the

patient too much inconvenience.

As discussed earlier, the boundary method can reduce noise in transmission measurements. However, in certain cases, it will not necessarily reduce the noise level in the final PCT images, because random noise in the emission scan also contributes to the noise level of PCT images (2,4). The boundary method improves a PCT image only if the image noise is not completely dominated by noise in the emission-scan data. These cases usually occur when the emission counts are below the anticipated levels due to unexpectedly low uptake of tracers in the organ of interest. Here the boundary method is not expected to help much in reducing the high noise level, because the noise is primarily due to the emission scan. The amounts of noise that are due to transmission scans and emission scans have been investigated for various combinations of transmission and emission counts (2,4), and the results can be applied easily to estimate how much the new method will improve the image noise in a particular case. If the predicted improvement is small, the method of using the measured ACFs is much easier, and the new method offers no advantage. Similarly, if the attenuation medium is uniform and has geometric shapes (e.g., cylindrical phantoms), the geometric AC is the ideal method to use and one need not make transmission measurements. However, when the attenuation medium has complex configurations and the transmission counts contribute significantly to the final image noise, the boundary method is expected to be most useful in improving PCT images.

With the development of newer scanners (17) that have higher efficiency and multiplane capabilities, it would appear that the boundary method is not needed because it is simpler merely to increase the transmission counts to reduce transmission noise. However, as has been shown (2), very high transmission counts are required to reduce the effect of transmission noise to a negligible level. Also, the fraction of PCT image noise that is due to transmission scan is not simply related to the total counts of transmission scan; it depends on the ratio between total counts in the transmission and emission scans (2,4). The ratio in turn is related to the relative scan times for transmission and emission and is completely independent of the efficiency of the scanners. In order to reduce the transmission-dependent fraction of image noise, a change in the relative scan times of the transmission scans and the emission scans would be required. It is not an efficient use of imaging time to spend a large portion of a patient's study on transmission measurements. In addition, newer scanners have higher imaging resolution, but it demands much higher count densities (as a third power of resolution) to achieve the same image noise level (7,18). Thus it is more critical to use the high efficiency of these scanners to increase the statistical quality of the emission image and to spend as little time as possible for transmission measurements.

So a method, such as the boundary method, is required to reduce the noise of transmission measurements. Otherwise, the high quality of the PCT image that is expected from these newer scanners would be degraded by the transmission noise. In other words, the boundary method is expected to become even more useful with newer scanners.

Since the boundary method can provide key object features from a transmission image, the method has the potential of reducing not only random noise but image artifacts due to calibration errors or object movement during transmission measurements. However, more study is required to explore this potential.

CONCLUSION

The boundary method is shown to be effective in reducing random noise in transmission measurements. For heart studies, the transmission scan time can be reduced by a factor of 3–10 with the method, and an improvement in image resolution is possible. For brain studies, because of the short scan time required by the boundary method, transmission scans can be performed routinely, and more accurate ACFs can be obtained without compromising on image noise levels.

ACKNOWLEDGMENTS

The authors thank Joann Miller, Francine Aguilar, and Ron Sumida for their invaluable technical assistance in carrying out the tomographic scans reported in this paper; Maureen Kinney and Gail Corso for typing the manuscript; and Lee Griswold for preparing the illustrations.

This work was supported by DOE Contract DE-AM03-76-SF-0012, NIH Grant R01-GM-24839-01, and USPH Grant No. 515654-01.

APPENDIX

Compensation of attenuation crossovers due to imaging resolution. In PCT, image resolution on the order of more than 1 cm in FWHM is quite comparable to the size of certain anatomical structures, such as the thickness of skull or the chest wall. In these cases, the attenuation coefficients derived from transmission images can deviate greatly from their true values (15). Also, there are significant crossovers of attenuation between adjacent structures or regions with different levels of attenuation coefficient. Theoretically these smoothing effects due to imaging resolution can be removed by deconvolving the image with the point spread function of the imaging system, but the relatively high noise in the PCT transmission images renders deconvolution completely impractical. Instead, an approximation method, as described below, has been used to compensate for the resolution effects on the average attenuation coefficients in regions that are enclosed by the boundaries determined by edge-finding techniques.

Assume that there are N separate regions in a slice and the attenuation coefficient is uniform within each region. Let μ_i denote the attenuation coefficient in Region i . If the slice is imaged by some system that has resolution $\text{FWHM} = w$, the average measured attenuation coefficient, m_i , in each region will not necessarily be equal to μ_i . Assume the imaging system is linear, then m_i and μ_i are linearly related as

$$m_i = \sum_{j=1}^N k_{ji} \mu_j, \quad i = 1, \dots, N$$

If the values of k_{ji} are known, those for μ_i can be obtained from the m_i values by solving the above set of linear equations.

For N regions of arbitrary size and shape, the k_{ji} values can be obtained by the following procedure. We construct an image of the known regions with $\mu_i = 1$ for $i = j$, and $\mu_i = 0$ for $i \neq j$, and apply a two-dimensional smoothing to the image to give an equivalent image resolution of $\text{FWHM} = w$; the average value in Region i of the smoothed image will then be the value of k_{ji} . Repeating the same procedure but each time selecting a different region j to construct an image, we can obtain all the k_{ji} values.

Thus, if the exact boundaries of the regions are known, the true attenuation coefficients in each region can be obtained from the average values in the smoothed image. In other words, compensation of the crossover due to imperfect imaging resolution can be achieved.

REFERENCES

1. PHELPS ME: Emission computed tomography. *Semin Nucl Med* 7:337–365, 1977
2. HUANG S-C, HOFFMAN EJ, PHELPS ME, et al: Quantitation in positron emission computed tomography: 2. Effects of inaccurate attenuation correction. *J Comput Assist Tomogr* 3:804–814, 1979
3. PHELPS ME, HOFFMAN EJ, MULLANI NA, et al: Application of annihilation coincidence detection to transaxial reconstruction tomography. *J Nucl Med* 16:210–224, 1975
4. GULLBERG GT, HUESMAN RH: Emission and transmission noise propagation in positron emission computed tomography. *J Nucl Med* 20:609, 1979 (abst)
5. BERGSTROM M, BOHM C, ERICSON K, et al: Corrections for attenuation, scattered radiation, and random coincidences in a ring detector positron emission transaxial tomograph. *IEEE Trans Nucl Sci* NS-27:549–554, 1980
6. ROSENFELD A: *Picture Processing by Computer*. New York, Academic Press, 1969, pp 95–100
7. PHELPS ME, HOFFMAN EJ, HUANG S-C, et al: ECAT: A new computerized tomographic imaging system for positron-emitting radiopharmaceuticals. *J Nucl Med* 19:635–647, 1978
8. PHELPS ME, HUANG SC, HOFFMAN EJ, et al: Tomographic measurement of local cerebral glucose metabolic rate in humans with (F-18)2-fluoro-2-deoxy-D-glucose: Validation of method. *Ann Neurol* 6:371–388, 1979
9. HUANG S-C, PHELPS ME, HOFFMAN EJ, et al: Noninvasive determination of local cerebral metabolic rate of glucose in man. *Am J Physiol* 238:E69–E82, 1980
10. MAZZIOTTA J, PHELPS ME, MILLER J, et al: The metabolic map of the unstimulated human brain in transverse and coronal section. *J Comput Assist Tomogr* 4:701, 1980 (abst)
11. SCHELBERT HR, PHELPS ME, HOFFMAN EJ, et al: Regional myocardial perfusion assessed with N-13 labeled ammonia and positron emission computerized axial tomography. *Am J Cardiol* 43:209–218, 1979
12. GOULD KL, SCHELBERT HR, PHELPS ME, et al: Noninvasive assessment of coronary stenoses with myocardial perfusion imaging during pharmacologic coronary vasodilation. *Am J Cardiol* 43:200–208, 1979
13. GALLAGHER BM, ANSARI A, ATKINS H, et al: Radiopharmaceuticals XXVII. ^{18}F -labeled 2-deoxy-2-fluoro-D-glucose as a radiopharmaceutical for measuring regional myocardial glucose metabolism in vivo: Tissue distribution and imaging studies in animals. *J Nucl Med* 18:990–996, 1977.
14. PHELPS ME, HOFFMAN EJ, SELIN C, et al: Investigation of [^{18}F]2-fluoro-2-deoxyglucose for the measure of myocardial glucose metabolism. *J Nucl Med* 19:1311–1319, 1978

15. HOFFMAN EJ, HUANG S-C, PHELPS ME, et al: Quantitation in positron emission computed tomography: 1. Effect of object size. *J Comput Assist Tomogr* 3:299-308, 1979
16. *Clinical Dosimetry*. NBS Handbook 87. Washington DC, U.S. Government Printing Office, 1963
17. HOFFMAN EJ, PHELPS ME, HUANG SC, et al: A new tomograph for quantitative positron computed tomography of the brain. *IEEE Trans Nucl Sci* NS-28:99-103, 1981
18. BUDINGER TF, DERENZO SE, GULLBERG GT, et al. Emission computed assisted tomography with single-photon and positron annihilation photon emitters. *J Comput Assist Tomogr* 1:131-145, 1977

SNM BOOKS

SINGLE PHOTON EMISSION COMPUTED TOMOGRAPHY and Other Selected Computer Aspects. Ron R. Price, David L. Gilday, and Barbara Y. Croft, Eds. This volume, which was published in 1980, includes an overview of single photon emission computed tomography and numerous papers that describe and evaluate specific systems and techniques. Papers cover such topics as Anger Cameras; seven-pin-hole and slant-hole collimators; brain, cardiac, and gated blood-pool studies; and the BICLET and SPECT systems. (SNM members: \$18.00 + \$2.50 postage and handling; list price \$27.00)

NUCLEAR MEDICINE REVIEW SYLLABUS. Peter T. Kirchner, Ed. This well-indexed volume is a comprehensive review of the major scientific and clinical advances that have occurred *since the early 1970's*. The chapters include Radiopharmacology, Instrumentation, Radiation Effects and Radiation Protection, Cardiovascular, Central Nervous System, Endocrinology, Gastroenterology, Genito-Urinary System, Hematology-Oncology, Pulmonary, Radioassay, and the Skeletal System and were prepared by more than fifty recognized authorities in their fields. (\$30.00 + \$2.50 postage and handling.)

RADIOPHARMACEUTICALS II. PROCEEDINGS OF THE 2nd INTERNATIONAL SYMPOSIUM ON RADIOPHARMACEUTICALS. Vincent J. Sodd, David R. Allen, Dennis R. Hoogland, and Rodney D. Ice, Eds. This 809 page volume is a complete compilation of papers from the 1979 International Symposium, including a Keynote Address by former AEC Chairperson Dixy Lee Ray and a panel discussion entitled "International Regulatory Affairs Relating to Radiopharmaceuticals." Chapters cover such topics as quality control, organic and inorganic radiopharmaceuticals, functional imaging, RIA, pharmacokinetics, and various body systems. (\$40.00 + \$2.50 postage and handling. **Special Offer!** Buy *Radiopharmaceuticals II* for \$40.00 and get *Radiopharmaceuticals* for only \$10.00 + \$2.50 each postage and handling!)

Other books available from the Society are *THE HERITAGE OF NUCLEAR MEDICINE* (\$14.50), *NUCLEAR CARDIOLOGY: SELECTED COMPUTER ASPECTS* (\$12.50), *NUCLEAR MEDICINE IN CLINICAL PEDIATRICS* (\$22.50), *SEMICONDUCTOR DETECTORS IN THE FUTURE OF NUCLEAR MEDICINE* (\$7.50), *TOMOGRAPHIC IMAGING IN NUCLEAR MEDICINE* (\$12.00), and the *NUCLEAR MEDICINE SCIENCE SYLLABUS* (\$30.00). For ordering and additional information please contact: Book Order Department, Society of Nuclear Medicine, 475 Park Avenue South, New York, NY 10016 or phone (212) 889-0717.